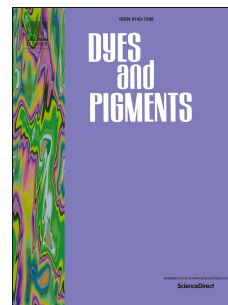# Accepted Manuscript

Photoinduced processes of adsorbed and associated dye molecules in mesoporous titania coatings

Borbála Tegze, Emőke Albert, Bálint Fodor, György Sáfrán, Zoltán Hórvölgyi

Please cite this article as: Tegze Borbá, Albert Emő, Fodor Bá, Sáfrán Gyö, Hórvölgyi Zoltá, Photoinduced processes of adsorbed and associated dye molecules in mesoporous titania coatings, *Dyes and Pigments* (2019), doi: https://doi.org/10.1016/j.dyepig.2019.04.017.

Photoinduced processes of adsorbed and associated dye molecules in mesoporous titania coatings

Borbála Tegze[a], Emőke Albert[a], Bálint Fodor[b], György Sáfrán[c], Zoltán Hórvölgyi[a]*

[a] Budapest University of Technology and Economics, Faculty of Chemical Technology and Biotechnology, Department of Physical Chemistry and Materials Science, Centre for Colloid Chemistry, H-1521 Budapest, Budafoki út 6-8, Hungary
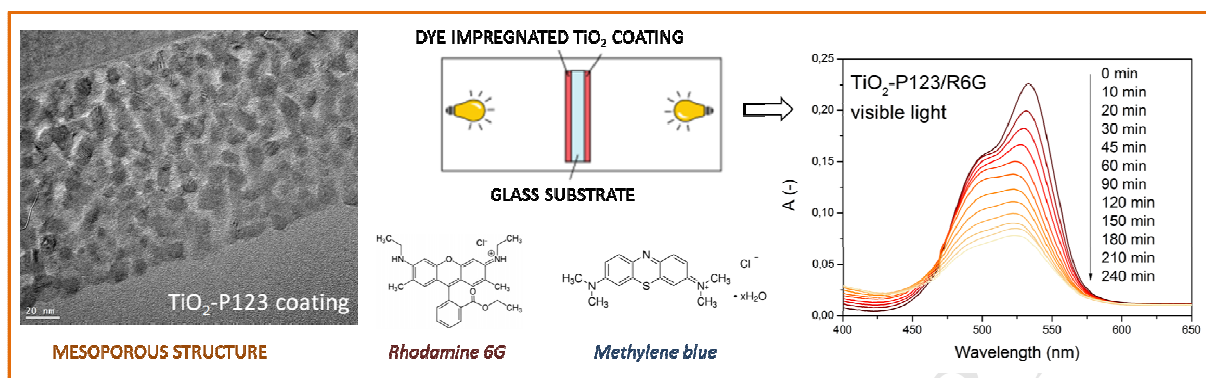
[b] Semilab Semiconductor Physics Laboratory Co. Ltd., H-1117 Budapest, Hungary

[c] Centre for Energy Research, Institute for Technical Physics and Materials Science, H-1121 Budapest, Hungary

*Corresponding author: E-mail: zhorvolgyi@mail.bme.hu, Phone: +36-1-463 2911, Fax: +36-1-463 3767

Declarations of interest: none.

Graphical Abstract

Highlights

- Sol-gel synthesis of mesoporous titania coatings with different pore structures
- Dye association in pores depends on the pore sizes and pH of dye solution
- Dye association influences the photodegradation process
- Monomers show higher photodegradation rates than associated dye molecules
- Photodegradation kinetics at air-solid interface evaluated by models from literature

Abstract

Studying photodegradation in porous semiconductor thin coatings by optical spectroscopy measurements (using dye model molecules) at the air-solid interface can be a simple model system relevant for such applications as self-cleaning coatings and dye-sensitized solar cells. Still, the interpretation of the results can be difficult, which is further complicated by the possibility of dye association processes. In this work, mesoporous titania coatings with different pore structures of 77-291 nm thickness and 30-45% porosity were prepared by sol-gel dip coating method on solid substrates, and impregnated in dye (rhodamine 6G, methylene blue) solutions. Dye photodegradation was studied under UV and visible light at the air-solid interface. Dye molecules adsorbed in the pore structure in monomer and associated forms: it was found that the association and dynamics of dye molecules depended on the pore sizes, and had an important role during photodegradation processes. Dye association was observed to occur during irradiation in the coatings with the highest pore thickness, while this process

was inhibited in the coatings containing smaller pores. Associated forms of the investigated dyes showed higher photostability compared to the monomer. The degradation of rhodamine 6G monomers showed a two-step first order reaction, as interpreted by the Julson-Ollis model.

Keywords: sol-gel coating, mesoporous titania, photodegradation, dye association, dye adsorption

1. Introduction

TiO_2 is a widely used photocatalytic and photovoltaic material, as it is non-toxic, low-cost, and shows high photoactivity. Its applications include air and water purification, solar cells *etc*. [1–7] In many studies dyes are used as model materials in photocatalytic measurements [8–11], as they are easily detected by optical spectroscopic methods; furthermore, dye-semiconductor systems have practical importance in the fields of dye-sensitized solar cells (DSSCs) [4,12], and waste water treatment in the textile industry where dyes are major pollutants [13–15]. Most studies measure the absorbance decrease of dye solutions containing photoactive materials under ultraviolet (UV) or visible light [9,16–21], and only a fraction of the literature describes measurements on the air-solid interface, which can provide a simple model system and can be especially important for self-cleaning coatings [22–27]. Photodegradation studies at the air-solid interface have the advantage of being a simpler model system, compared to the photodegradation studies carried out in solutions, where *e.g.* the diffusion of molecules to the surface also has an important role in the process. On the other hand, this model also has disadvantages: the dye concentration, the absorbance spectrum of the coated samples and hence, the photodegradation of adsorbed species is harder to interpret compared to that of the solutions.

A well-defined layer of dye molecules can be formed at the solid surface of particles or mesoporous materials by adsorption from dye solutions. Not much attention has been paid to

the physical state and the organization of adsorbed molecules trapped in the confined spaces of porous photoactive materials, especially in coatings, as related to the photodegradation rates and kinetics [23–26]. Dye molecules can be adsorbed on the semiconductor surface as monomers or as their aggregated forms [28]. It can be expected that the aggregated forms (*e.g.* dimers) have different photostability and show different degradation rates and kinetics than the monomer form [26]. Studying the photostability of the monomer and different associated dye molecules is also important in the fields of dye lasers, fluorescent dye probes and anti-corrosive coatings [29–32]. Moreover, the air-solid model system provides a unique possibility for studying the photostability of monomer and associated molecules independently from each other, due to the lack of real dynamic equilibrium at the air-solid interface in the porous system.

The aim of our paper is to investigate the behaviour of dye molecules in a thin layer model system: in the confined spaces of mesoporous titania coatings, with the main focus on the relationship between dye association and photodegradation processes. We are interested in how dye association and the pore structure can influence the photodegradation rate and kinetics. Furthermore, our aim was to investigate whether photodegradation in very thin mesoporous coatings at the air-solid interface can be reliably studied by optical spectroscopy methods. For this reason, the results were interpreted by help of previous findings in the literature, including kinetics models, conducted on similar air-solid model systems. Three different types of titania coatings were prepared, with different pore size distribution and porosity, in order to better understand how the relevant parameters influence the dye association, adsorption and photodegradation processes. Rhodamine 6G and methylene blue were chosen as the investigated cationic dyes, since both are known for significant dye association ability in porous systems. A more in-depth study was carried out on rhodamine 6G

dye, which also shows dye sensitization, and thus the degradation process was investigated under both UV and visible light.

2. Experimental

All reagents were of analytical grade and used without any further purification. Materials used for the precursor sol synthesis: Tetraethyl orthosilicate (TEOS, 99%, Merck), Titanium(IV) butoxide (for synthesis, 98%, Merck), titanium(IV) isopropoxide (98+%, Acros Organics), ethanol (EtOH, a.r., >99.7%, Reanal), 2-propanol (2-PrOH, a.r., >99.7%, Reanal), nitric acid (HNO$_3$, special grade, 65%, Lach-Ner), hydrochloric acid (HCl, 37%, Reanal), acetylacetone (AcAc, 99>%, Acros Organics), cetyltrimethylammonium bromide (CTAB, cationic surfactant, 99+%, Acros Organics), Pluronic P123 (P123, average mol wt 5800, 99%, Sigma Aldrich), polyvinylpyrrolidone (PVP, average mol wt 40000, Sigma Aldrich) and distilled water (H$_2$O, 18.2 MΩcm, purified by Millipore Simplicity 185 filtration system). Microscope glass slides (76 × 26 × 1 mm, Thermo Scientific, Menzel-Gläser), silicon wafers (Siegert, (100), p-type, 1-30 cm, prime grade) and quartz glass slides (25 × 30 × 1.05 mm, Optilab Kft., Suprasil 1) were used as solid substrates of the coatings. Solid substrates were cleaned using 2-propanol (2-PrOH, a.r., >99.7%, Reanal) and distilled water (H$_2$O, 18.2 MΩcm, purified with a Millipore Simplicity 185 filtration system).

The dyes used during the photocatalytic measurements were rhodamine 6G (R6G, 95%, Sigma Aldrich) and methylene blue (MB, >95%, Reanal) (Appendix Fig. A.1). R6G is a cationic dye with a size of *ca.* 1.38 nm × 1.15 nm × 0.9 nm [33]. Its molecule is not planar: one aromatic group is perpendicular to the main plane of the molecule. MB is a cationic dye with a size of *ca.* 1.38 nm × 0.59 nm [34], and a planar molecular structure.

2.1 Synthesis of precursor sols

5

Titania and silica coatings were prepared via sol-gel process on solid substrates (glass, silicon). In the case of glass substrates, first a compact silica film was deposited on the glass, and then the TiO_2 film was coated onto the surface in a second step. The silica coating was used as a protective barrier between the glass and the titania film to prevent ion (mainly Na^+) migration from the glass into the titania, as Na^+ ions decrease the photoactivity [35].

2.1.1 Silica precursor sol

Silica precursor sol was prepared via the acid catalysed controlled hydrolysis of TEOS in ethanolic media. HCl was used as catalyst during the synthesis of the precursor sol. The molar ratios for TEOS : EtOH : HCl : H_2O were $1 : 4.75 : 7.2 \times 10^{-4} : 4.00$.

The obtained mixture was stirred for 1 h at room temperature. The resulting sol was completely clear and colourless.

2.1.2 TiO_2-CTAB precursor sol

Titania precursor sol containing CTAB template was prepared via the nitric acid catalysed controlled hydrolysis of titanium(IV) butoxide in ethanolic media. The molar ratios for titanium(IV) butoxide : EtOH : HNO_3 : H_2O : CTAB were $1 : 27.74 : 0.39 : 1.54 : 0.124$.

The CTAB template was dissolved in ethanolic media, then titanium(IV) butoxide, nitric acid and distilled water were added to the solution, and the mixture was stirred for 2 h at 60 °C. The resulting sol was completely clear and had a slightly yellow colour.

Titania coatings prepared using the precursor sol will be referred to as TiO_2-CTAB type samples.

2.1.3 TiO_2-P123 precursor sol

Titania precursor sol containing P123 template was prepared by dissolving the P123 template in ethanol, adding titanium(IV) isopropoxide, then acetylacetone. After stirring the solution for 1 h at room temperature (RT), distilled water was added; followed by 30 min of ultrasound and a further 1 h stirring at RT. The resulting sol was completely clear and had a yellow colour. The molar ratios for titanium(IV) isopropoxide : EtOH : acetylacetone : H_2O : P123 were 1 : 33.80 : 0.97 : 2.19 : 0.034.

Titania coatings prepared using the precursor sol will be referred to as TiO_2-P123 type samples.

2.1.4 TiO$_2$-PVP precursor sol

Titania precursor sol containing PVP template was prepared by dissolving PVP in ethanol, adding distilled water, HCl solution and titanium(IV) butoxide, and stirring the obtained mixture for 2 h at RT. The resulting sol was completely clear and had a slightly yellow colour. The molar ratios for titanium(IV) butoxide : EtOH : HCl : H_2O : PVP were
1 : 8.03 : 0.051 : 0.91 : 2.5×10^{-5}.

Titania coatings prepared using the precursor sol will be referred to as TiO_2-PVP type samples.

2.2 Preparation of coatings

Sol–gel coatings on solid substrates were prepared from the precursor sols by the dip coating method. Microscope glass slides and in certain cases silicon (100) wafers and quartz glass slides were used as solid substrates for layer deposition. Prior to coating deposition solid substrates were cleaned with 2-propanol and distilled water, and dried at RT. Silica thin film was used as a barrier layer between the glass substrate and the TiO_2 thin film. In case of TiO_2 film deposition on silicon substrates and quartz glass slides no silica barrier layer was used.

Cleaned and dried substrates were immersed in the precursor sol and pulled out with a constant speed of 6 cm min^{-1} (silica and TiO$_2$-PVP precursor sols) or 12 cm min^{-1} (TiO$_2$-CTAB and TiO$_2$-P123 precursor sols), using a dip coater device (Plósz Engineering Ltd., Hungary).

The deposited films were annealed in an oven (Nabertherm B170) at 450 °C for 30 min in the case of TiO$_2$-CTAB samples, and at 480 °C for 60 min in the case of TiO$_2$-P123 and TiO$_2$-PVP samples.

2.3 Dye adsorption and desorption

Rhodamine 6G and, in some experiments, methylene blue dye molecules were adsorbed into the pore structure of titania coatings from aqueous solutions. The dyes were adsorbed from 10^{-3} M aqueous solution at pH = 10 (pH adjusted with NH$_3$). During preliminary experiments, no significant adsorption was seen at the lower pH value of the as-prepared 10^{-3} M aqueous solutions (pH = 6 for R6G solutions and pH = 4.5 for MB solution), while the dye molecules were adsorbed on the surface in the highest amount in the range pH = 9-11. A pH adjustment with NH$_3$ was necessary for the adsorption, as at this high pH value the titania surface is negatively charged, and the positively charged dye cations readily adsorb onto it. [13,23]

The impregnation was carried out with immersion and withdrawal speeds of 10 cm min^{-1}, and an immersion time of 2 min using a dip coater. Following the impregnation, the samples were rinsed with distilled water to avoid excessive dye accumulation on the outer surface of the sample, and dried at room temperature.

In order to determine the number of dye molecules adsorbed in the coatings, dye desorption measurements were carried out by placing the dye impregnated samples in 30 mL of distilled water. After keeping them immersed for 1 h (equilibrium was reached), the samples were

8

taken out, and the absorbance spectra of the resulting dye solutions were measured between 400-800 nm.

2.4 Characterization methods

2.4.1 Optical characterization of coatings by UV-Vis spectroscopy

The optical properties of the prepared coatings on glass substrates were investigated by UV–Vis spectroscopy using a Specord 200–0318 spectrophotometer. Transmittance spectra of the samples were measured in the wavelength range of 350–1100 nm, using 1 nm resolution and a scanning speed of 10 nm s^{-1}.

The effective refractive index (at 632.8 nm) and thickness values of the coatings were determined by applying thin layer optical models to the obtained transmittance data, as described in our previous publications [32,36,37]. The thin layer optical model [38] used for the fitting procedure supposes identical homogeneous layers of the same material on both sides of the transparent substrate, and the light arriving at the sample at a perpendicular angle of incidence. The fitting procedure used a Levenberg–Marquardt algorithm. For silica/TiO$_2$ two-layered samples, a two-layered optical model was applied. Before the fitting procedure, the transmittance spectra of the coatings were corrected using the spectra of the glass substrates, in order to eliminate the effect of their weak absorption in the measured wavelength range. The porosity of titania coatings was estimated from the effective refractive index values using the Lorentz–Lorenz formula [39].

The absorbance spectra of the dye impregnated samples were measured in the wavelength range of 400–800 nm, using the same resolution and scanning speed as before.

2.4.2 Ellipsometric porosimetry measurements

TiO$_2$-P123 and TiO$_2$-PVP type porous titania coatings deposited on Si substrates were investigated by ellipsometry and ellipsometric porosimetry characterization methods, using a Semilab's PS-2000 device. Ellipsometry can be used to determine the optical properties, film thickness and total porosity values of the samples. Ellipsometric porosimetry is a coupled measurement method, in which the vapour adsorption in the pores can be monitored by spectroscopic ellipsometry. By recording the adsorption and the desorption isotherms, the pore size distribution (for open porosity) of the sample can be determined. The pore size distribution can be calculated based on the modified Kelvin equation in the case of mesopores. Ellipsometric porosimetry measurements were carried out at the angle of incidence of 60° in the wavelength range of 275.6 – 968.8 nm, using toluene as the adsorptive material. Before the measurement, the samples were heated up to 448 K for 20 min. The adsorption isotherms were taken at 294 K. The thickness and the effective refractive index of the coatings were determined by applying the Tauc–Lorentz oscillator model successfully in the full wavelength range.

The ellipsometric porosimetry results of TiO$_2$-CTAB type titania coatings shown here are taken from one of our previous publications [40]. The coating preparation and ellipsometric porosimetry characterization were done the same way as described here.

2.4.3 Transmission electron microscopy measurements

Transmission electron microscopic (TEM) and high-resolution transmission electron microscopic (HRTEM) investigations of the titania samples were carried out by 300 kV JEOL 3010 HRTEM, with a point resolution of 0.17 nm. For TEM characterization, cross-sectional TEM (XTEM) samples of the TiO$_2$-CTAB, TiO$_2$-P123 and TiO$_2$-PVP were prepared by mechanical and ion beam thinning techniques, as reported previously [41].

2.4.4 Photodegradation measurements

Photodegradation experiments were carried out at the air-solid interface. R6G and MB dye impregnated coatings were irradiated with UV and visible light.

57W LED light bulbs (GE 93845, spectrum: emitting light from 420 to 780 nm with a maximum at 600 nm) were used as a visible light source, and 20W UV-A light bulbs (Sylvania BL368, light emittance maximum at 368 nm) were used as UV radiation source. Two light bulbs and the measured samples were placed in an irradiation house; the samples were positioned halfway between the two light sources with the light arriving at the coating perpendicularly and from both sides, with an incident light intensity of 0.47 mW cm^{-2} and 0.20 mW cm^{-2} in the case of the visible and UV light source, respectively. The distance between the sample and the light source was 23 cm.

Dye photodegradation was monitored by measuring the absorbance of the dye impregnated coatings after t time of UV or Vis irradiation in the 400-700 nm wavelength range. The absorption spectra were measured by an Analytic Jena Specord 200–0318 type UV-Vis spectrophotometer. The absorption spectra were corrected with the absorbance values measured before the dye adsorption. The absorbance decrease of different samples is compared by calculating A/A_0 where A and A_0 are the absorbance at a given wavelength after t time of irradiation and before irradiation, respectively. The studied wavelength values were around 533 nm (measured at the maximum of the absorbance spectra) for R6G dye monomer, 500 nm for R6G dimer form, 655 nm for MB dye monomer and 550 nm for MB trimer form. In certain cases the quantum efficiency and quantum yield were also calculated. In reference measurements, dye impregnated titania samples were kept in dark, and dye impregnated porous silica coatings were irradiated with the UV source for the same time intervals as used in the photodegradation measurements: the absorption peak of the dye did not show significant change in either case. In comparison, MB impregnated titania coatings under UV

irradiation and R6G impregnated samples under both UV and visible light showed considerable absorbance decrease as a result of the photoactivity of the titania coatings.

3. Results and discussion

The results are described in the following three sections: characterization of as-prepared coatings, dye-adsorption and photodegradation. A thorough investigation was carried out on R6G impregnated titania coatings, the dye adsorption and the photodegradation of the dye molecules were studied. Further experiments were carried out on MB impregnated coatings, in order to broaden the information given by the results of the R6G dye measurements.

3.1 Characterization of as-prepared coatings

The porous TiO_2 coatings prepared on SiO_2 coated solid substrates were characterized by UV-Vis spectroscopy, HRTEM, ellipsometry and ellipsometric porosimetry methods.

3.1.1 Optical characterization of coatings by UV-Vis spectroscopy

Characteristic transmittance spectra of the samples can be seen in Appendix Fig. A.2. The silica coatings show higher transmittance than the uncoated glass substrates for the whole studied wavelength range, which can be attributed to the lower effective refractive index values of the investigated samples (see Table 1) compared to the bare glass substrate ($n_{glass} = 1.52$). The titania coated two-layered samples show lower transmittance (T = 70-90%), due to the higher effective refractive index of titania. The differences in the transmittance spectra of the different types of SiO_2/TiO_2 samples are due to the different layer thickness, refractive index values and pore structures of the titania thin films.

Optical parameters and layer thickness values of the prepared coatings were determined by applying fitting procedures according to an appropriate thin film optical model. The layer thickness, effective refractive index and porosity values are presented in Table 1. Porosity values of the titania coatings were estimated from the effective refractive index of the layers,

using the Lorentz-Lorenz equation. The reduced χ^2 values of the performed fitting were in the range of 10^{-7} to 10^{-8}, which shows a good agreement between the measured and the fitted spectra. It was found that all three types of titania coatings have similar properties: very low film thickness, between 80-300 nm; and porosity in the 30-45% range.

Table 1: Refractive index (n), film thickness (d) and porosity (P) values of silica and porous titania coatings determined by UV-Vis spectroscopy

	n	d (nm)	P (%)
SiO_2	1.448 ± 0.005	190 ± 5	-
TiO_2-CTAB	1.812 ± 0.014	77 ± 2	30 ± 1
TiO_2-P123	1.600 ± 0.015	116 ± 3	44 ± 1
TiO_2-PVP	1.819 ± 0.010	299 ± 8	29 ± 1

3.1.2 Characterization of coatings by ellipsometric porosimetry

The film thickness, refractive index, porosity values and pore radius distribution of titania coatings were determined by ellipsometry and ellipsometric porosimetry measurements. As shown in Table 2, the TiO_2-CTAB type samples contained the narrowest pores, with a characteristic pore thickness of 5.0 nm (determined from desorption). Both TiO_2-PVP and TiO_2-P123 samples have higher pore sizes compared to TiO_2-CTAB, and their characteristic pore thickness values are similar to each other: 8.2 nm and 9.0 nm, respectively. As shown in Appendix Fig. A.3, the TiO_2-PVP coatings contain slightly bigger pores compared to TiO_2-P123 samples, according to the adsorption measurement. The results show that we were able to control the pore sizes in the titania coatings by changing the sol composition and the template molecules. TiO_2-PVP coatings have a lower specific surface area than TiO_2-P123 samples.

The refractive index, film thickness and porosity values of the coatings are in good agreement with the values determined by the optical model fitting procedure of the transmittance spectra (see Table 1).

13

Table 2: Pore radius (r_{ads}, r_{des} for adsorption and desorption measurements), porosity, specific surface area, film thickness (d) and refractive index (n) values of the titania coatings determined by ellipsometric porosimetry measurements. The values of TiO$_2$-CTAB samples are taken from a previous publication [40].

	Mesopores		Micropores		Porosity (%)	Specific surface area (m^2 cm^{-3})	d (nm)	n
	r_{ads} (nm)	r_{des} (nm)	r_{ads} (nm)	r_{des} (nm)				
TiO$_2$-CTAB	3.4 ± 0.0	2.5 ± 0.1	0.84 ± 0.01	0.60 ± 0.06	25 ± 0	689 ± 8	82	1.823
TiO$_2$-PVP	6.3 ± 0.0	4.1 ± 0.2	0.65 ± 0.01	1.50 ± 0.00	30 ± 1	761 ± 31	297 ± 1	1.806 ± 0.004
TiO$_2$-P123	6.1 ± 0.2	4.5 ± 0.1	0.74 ± 0.04	0.82 ± 0.59	42 ± 2	1093 ± 59	124 ± 1	1.576 ± 0.017

3.1.3 High Resolution Transmission Electron Microscopy measurements

The structure and morphology of TiO$_2$-CTAB, TiO$_2$-P123 and TiO$_2$-PVP porous titania samples were investigated by TEM and HRTEM methods. Fig. 1 shows the cross-sectional images of the samples. The film thickness values determined from the images (74 nm for TiO$_2$-CTAB samples; 126 nm for TiO$_2$-P123 samples; 292 nm for TiO$_2$-PVP samples) are in good agreement with the UV-Vis spectroscopy and ellipsometry results (Table 1 and 2). According to both the contrast features of the conventional cross sectional TEM and lattice resolution HRTEM images, all samples exhibit crystalline TiO$_2$ grains more or less separated by pores. The TiO$_2$-CTAB samples show an irregular pore structure, different from the ordered cylindrically shaped pores that can be achieved using the micelle formation of CTAB surfactants in *e.g.* porous SiO$_2$ thin film preparation [32,42,43]. It appears that during sol synthesis relatively large titania particles were formed, and this caused an irregular structure with the pores forming as voids between the particles. The other two types of coatings showed similar structures but with different titania particle- and pore size distribution. The TiO$_2$-CTAB and TiO$_2$-P123 pore structure appears to be more unified compared to the less homogeneous TiO$_2$-PVP structure. The pore size values of TiO$_2$-CTAB samples are between

2 nm and 5 nm, with a small amount of bigger pores (at most 6 nm in size), while the titania particles have sizes between 5 nm and 10 nm. TiO_2-P123 samples contain *ca.* 10 nm sized particles (sizes between 6-15 nm) with differently sized voids between them (mostly 3-6 nm in size, up to 8 nm). The HRTEM images of TiO_2-PVP samples show an irregular structure made of 10-20 nm sized particles, and pore thicknesses up to more than 10 nm. Both the particle sizes and the pore thickness values are the highest in the TiO_2-PVP samples (Fig. 1). HRTEM images and their Fast Fourier Transforms (FFT) were applied to reveal the crystal phase of the titania films (Fig. 1b-d). The lattice spacing measurements were calibrated to the resolved (111) period (0.311 nm) of the Si substrate (PDF 80-0018). Three polymorphs of TiO_2, rutile, anatase and brookite were suggested according to PDF data (database of International Centre for Diffraction Data). In all samples, the remarkable 0.352 nm ring of reflections may either correspond to the (101) lattice planes of bct anatase (PDF 84-1285) or the (210) planes of orthorhombic brookite (PDF 76-1937). However, in the FFTs the reflections of 0.29 nm representative for brookite are missing, therefore brookite can be excluded. In conclusion the titania coatings are built up of grains of anatase phase.
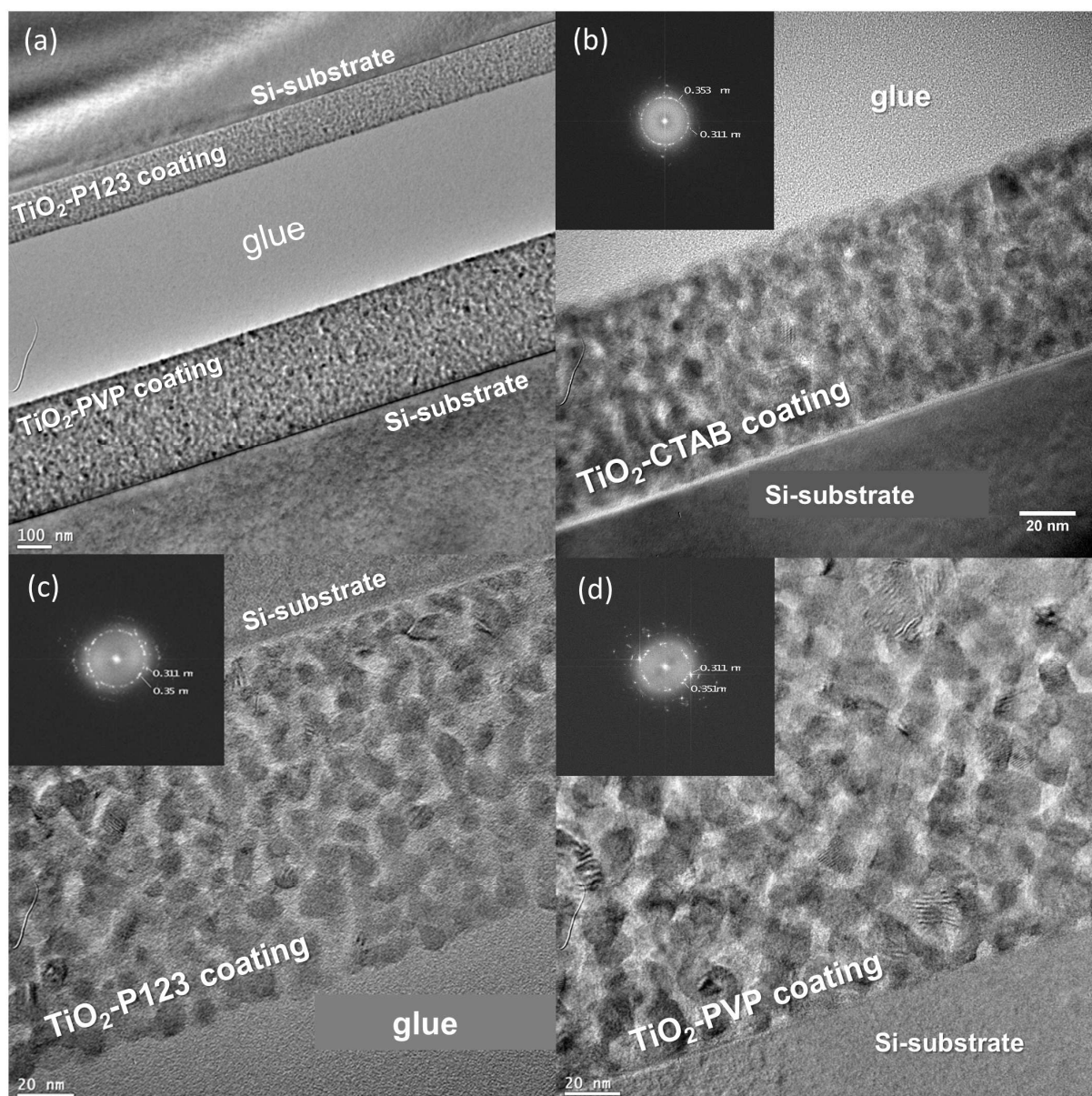
Fig. 1. Cross-sectional TEM images of TiO$_2$-P123 and TiO$_2$-PVP coatings (1a); and HRTEM images of TiO$_2$-CTAB (1b), TiO$_2$-P123 (1c), and TiO$_2$-PVP (1d) samples. The insets in 1b, 1c and 1d show the Fast Fourier Transforms of the respective HRTEM images.

3.2 Dye adsorption in the porous titania coatings

Rhodamine 6G and methylene blue dyes were adsorbed into the porous titania coatings from aqueous solutions. The dye impregnated coatings were characterized by UV-Vis spectroscopy.

3.2.1 UV-Vis spectroscopy of R6G impregnated coatings

The absorbance spectra of the dye impregnated coatings were measured by UV-Vis spectroscopy. Fig. 2a shows that no significant adsorption was seen at pH = 6 value of the as-prepared 10^{-3} M R6G aqueous solutions, while dye molecules adsorbed in the pores in a much higher amount at pH = 10, due to electrostatic attraction between the negatively charged surface and the cationic dye molecules. In further experiments, the dye was adsorbed from aqueous solutions of pH = 10.

Comparing the different dye impregnated porous samples, Fig. 2b shows that the TiO_2-PVP samples adsorbed a significantly higher amount of dye molecules compared to the TiO_2-CTAB and TiO_2-P123 samples, due to their higher film thickness. In Fig. 2d, it can be seen that TiO_2-PVP samples show the lowest absorbance normalized to the same 100 nm thickness, which can be due to the difference of specific surface area.

The number of dye molecules in the coating can be estimated as 2.0×10^{16} from dye desorption measurements carried out using TiO_2-P123 samples. This can be compared to the theoretically calculated maximum number of dye molecules adsorbed on the surface. If we assume adsorption with complete coverage on the surface, then from the specific surface value (1093 m^2 cm^{-3}) and the dye molecule size (equivalent spherical diameter = 1.6 nm [44]), it can be estimated that 1.9×10^{16} molecules would adsorb on the surface. As the two values are very close to each other, this suggests the complete coverage of the surface by dye molecules. However, it should also be taken into consideration that dimerization of the dye molecules also influences the surface coverage.

The absorbance spectra of the R6G solution and TiO_2/R6G samples show a maximum around 533 nm (531-534 nm), which is attributed to the monomer form, and a shoulder at 500 nm which corresponds to the H-dimer. The absorption band shape, which is related to the amount of dimers and monomers, is different in solution and for each type of porous coating (Fig. 2c).

17

As it can be seen in Fig. 2c, the number of dimers compared to the monomers (the dimer-to-monomer molar ratio calculated from the absorbance values) is lower in the coatings than in the 5×10^{-4} M aqueous solution. Dye molecules presumably diffuse into the pores in monomer form, and there may be a competition between the monomer-monomer and monomer-surface interactions. Due to the monomer-surface attraction, the dimerization cannot take place intensively, although the small pore spaces can also facilitate the process. TiO$_2$-CTAB type samples show the highest dimer-to-monomer molar ratio, which can be explained by these samples containing the narrowest pores (d = 5 nm) out of all samples. In the confined space of the pores the dimerization may be facilitated, due to the proximity of molecules. This becomes more prominent for smaller pore sizes, and causes more dimers to be present in the TiO$_2$-CTAB samples than in the TiO$_2$-P123 and TiO$_2$-PVP samples which have higher pore sizes.
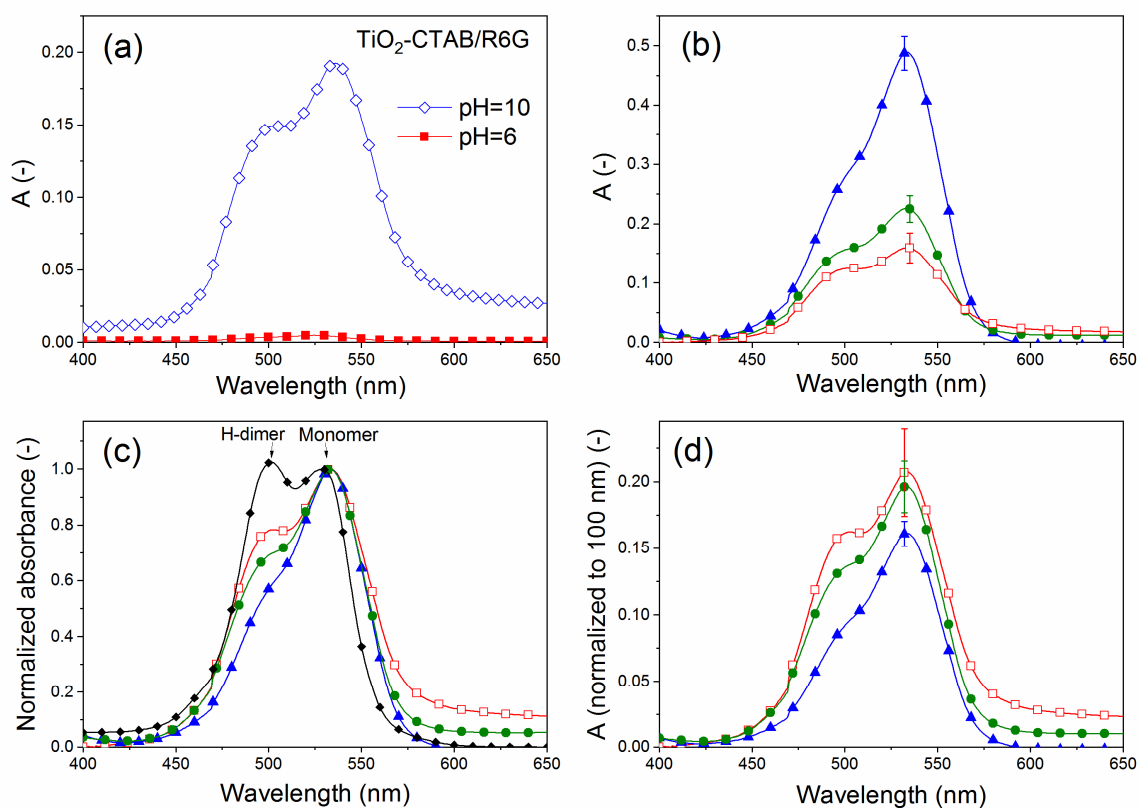

Fig. 2: Absorbance spectra of TiO$_2$-CTAB samples impregnated in dye solutions of different pH values (2a). Dye adsorption (from R6G solution of pH = 10) in the different porous coatings: absorbance (2b), normalized absorbance (to A$_{max}$ = 1) (2c) and absorbance

normalized to 100 nm film thickness (2d): R6G impregnated TiO$_2$-PVP (▲), TiO$_2$-P123 (●), TiO$_2$-CTAB (□) samples and 5×10^{-4} M R6G solution (♦).

3.2.2 UV-Vis spectroscopy of MB impregnated coatings

MB impregnated titania coatings were also investigated by UV-Vis spectroscopy (Fig. 3). Similarly to the results seen for R6G adsorption measurements, the TiO$_2$-PVP coatings were able to adsorb the highest amount of MB dye molecules (Fig. 3a), while once again these samples show the lowest absorbance when normalized to the same 100 nm thickness (Fig. 3b). It can be seen in Fig. 3c that MB shows markedly different absorption spectra in solution and in the impregnated coatings. Interestingly, dye association was increased in the pores compared to the solution, while the opposite was true for R6G molecules. The peak at 660 nm is attributed to MB monomer, the peak at 605 nm to the dimer, and the peak around 550 nm, that appears only in the dye impregnated coatings, is the trimer form [45]. The intensive trimer peak indicates higher dye concentration in the pores of the coatings. The dye molecules are mostly in trimer form, due to the relatively high equilibrium constants for the dimerization (2×10^3 M^{-1}) and trimerization steps (6×10^6 M^{-2}) for MB in water at 30 °C [46]), and the different behaviour of dye molecules in the confined space of the pore structures. Dimer molecules might also be present in a very small amount in the porous coatings, but their peak cannot be detected in the absorption spectra.

MB monomers are present in the highest amount compared to trimers in the TiO$_2$-CTAB type coatings. This can be explained by the pore sizes: these samples possess the smallest pore sizes, some of which are too small for the bigger trimer molecules, and this causes a higher monomer-to-trimer ratio (Fig. 3c). In comparison R6G dimers are still small enough to be able to be trapped in these pores (size of R6G molecule 1.38 nm $\times$ 1.15 nm $\times$ 0.9 nm [33]; size of MB molecule 1.38×0.59 nm [34]).

The results show that the amount of aggregated dyes adsorbed in a porous coating can be controlled with the pore sizes: aggregated forms will be in a higher amount with decreasing pore sizes up to a certain point, at which their amount will decrease as the pore sizes become too small for the associated forms.

An interesting phenomenon was also observed in the absorbance spectra of the MB impregnated samples: the monomer peak slowly decreased over time while the trimer peak slightly increased. An example is shown in Fig. 3d, of a TiO_2-PVP coating that was kept in dark for several days. This would suggest that monomer-to-trimer transformation occurred in the pore structure of the impregnated coatings.
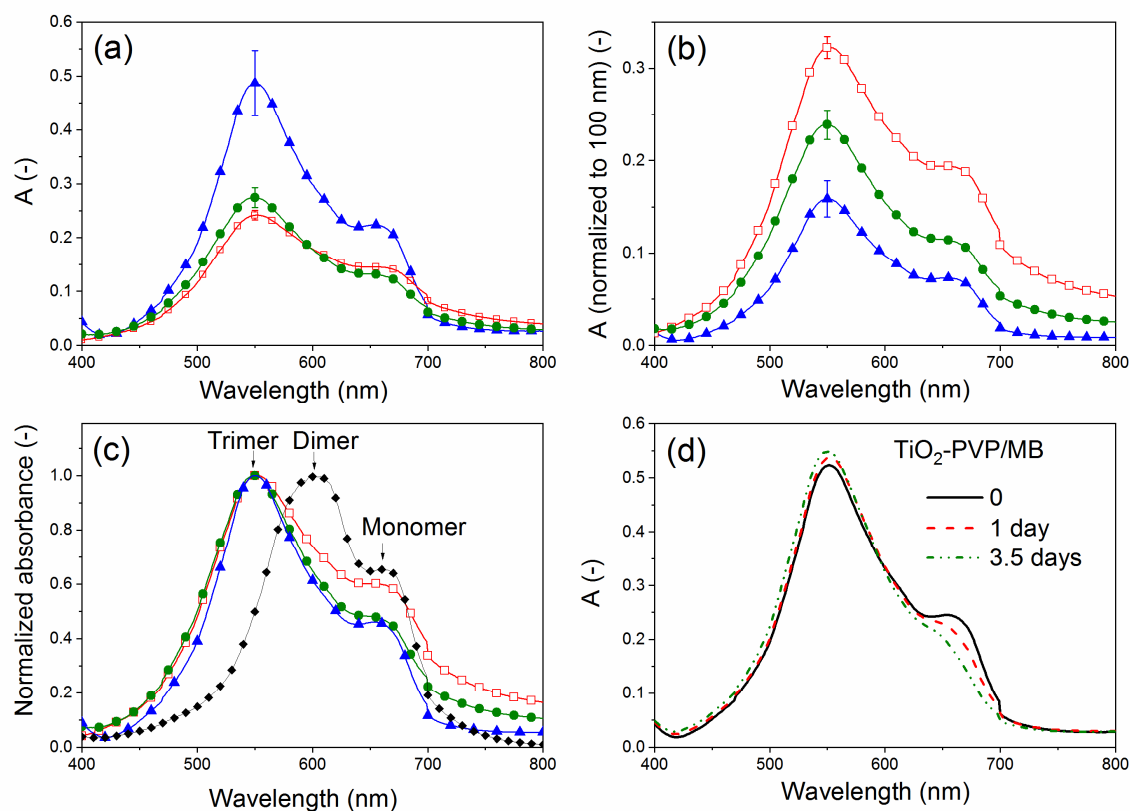

Fig. 3: Dye adsorption from MB solution of pH = 10 in the different porous coatings: absorbance (3a), absorbance normalized to 100 nm film thickness (3b) and absorbance normalized to A_{max} = 1 (3c): MB impregnated TiO_2-PVP (▲), TiO_2-P123 (●), TiO_2-CTAB (□) samples and 10^{-3} M MB solution (◆). Absorption spectra of MB impregnated TiO_2-PVP sample after impregnation (straight line), and after it was kept in dark for 1 (dashed line) and 3.5 (dash dot line) days (3d).

20

3.3 Dye photodegradation study

The photodegradation of two cationic dyes, rhodamine 6G and methylene blue, was studied in the pore structure of titania coatings. The TiO_2/MB system was only measured under UV light, while the TiO_2/R6G system was investigated in detail, under both UV and visible light irradiation. Photodegradation experiments under visible light were only carried out for R6G impregnated samples, as R6G dye was found to be capable of dye sensitization, while the MB dye could not sensitize the titania coatings. MB photodegradation was only observed under UV irradiation, while no discoloration of the samples occurred under visible irradiation.
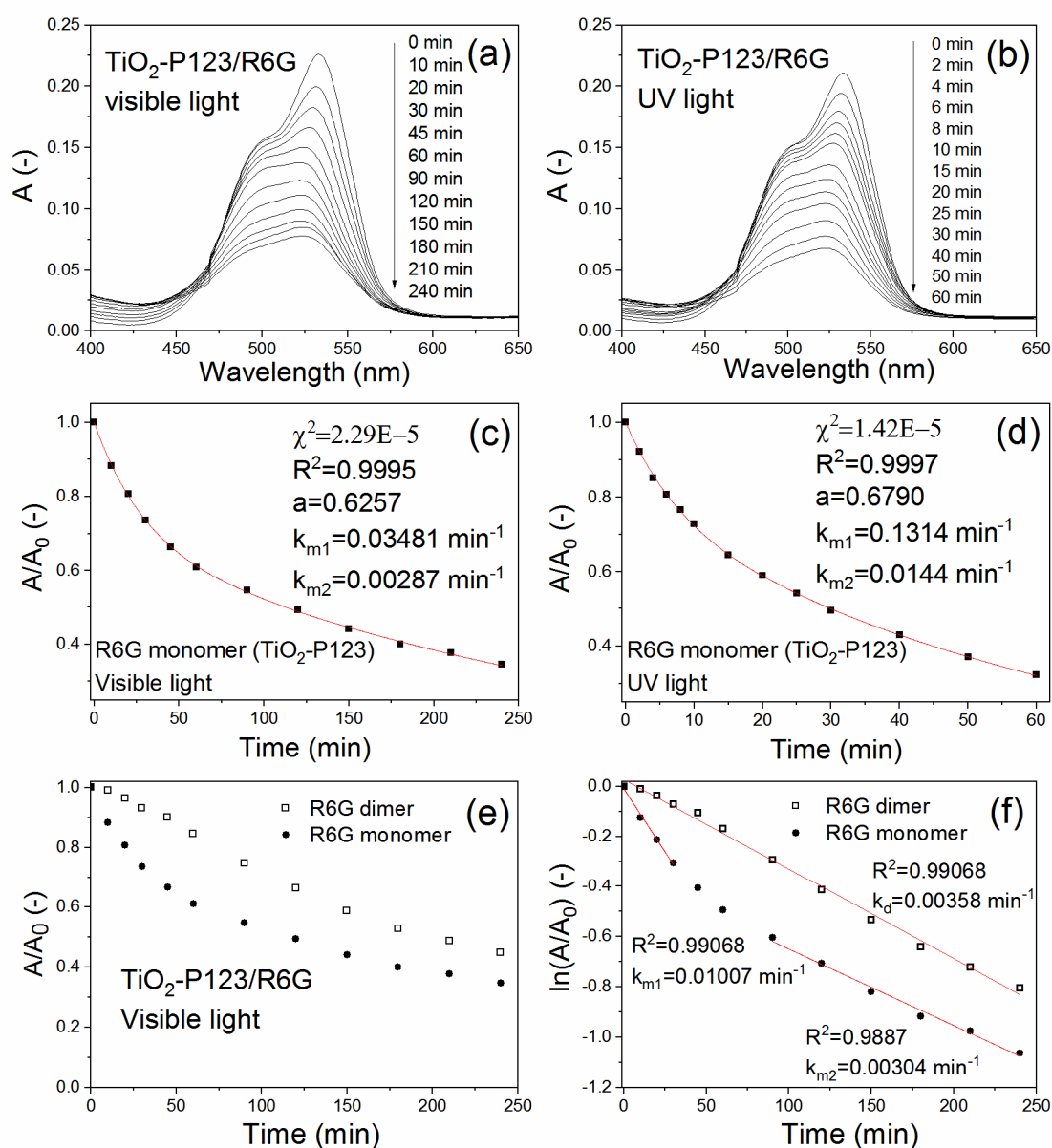
Fig. 4: Absorbance spectrum change of R6G impregnated TiO_2-P123 sample during visible (4a) and UV light illumination (4b); determination of the kinetics parameters for the monomer degradation by fitting the Julson-Ollis model equation to the data measured in visible (4c) and UV (4d) light; A/A_0 vs. time curves for monomers and dimers under visible light illumination (4e) and estimation of kinetics parameters by linear fitting, assuming pseudo-first order kinetics (4f). A/A_0 values were measured at the wavelength of maximum absorbance (monomer) and at 500 nm (dimer). The parameters seen in Fig. 4c, 4d and 4f are the ratio of molar absorptivities (a), degradation rate constant of dimers (k_d) and of monomers during the initial interval (k_{m1}) and during the second time interval (k_{m2}), and parameters that characterize the goodness of the fitting (χ^2, R^2).

3.3.1 Visible irradiation (R6G)

Fig. 4a shows the decreasing absorbance spectra of the R6G impregnated coatings

(TiO_2-P123) under visible light. The first change is a quick decrease in the monomer peak:

this first process occurring during the first 30 minutes of visible light illumination is observed

for all coatings. During this first, higher rate process the maximum wavelength attributed to

the monomer shifts to lower wavelength values, from 533 nm to 520 nm, which can be

attributed to the N-dealkylation of rhodamine 6G [48–50]. Dye photodegradation resulting in

CO_2 and H_2O is described in the literature [51] for intensive UV irradiation and can be

assumed to occur here at longer irradiation times, as the absorption decrease was significant

and irreversible.

As it can be seen in Fig. 4e, the A/A_0 values as a function of time for R6G monomers and

dimers show that the dimer degradation is slower than the monomer degradation. Similar

results were observed for all types of TiO_2 coatings. It is also apparent, that the monomer

degradation shows an initially faster degradation rate that slows down in time. The results can

be used to determine the degradation kinetics for R6G monomers and dimers. Several

different kinetics models have been used in the literature for dye degradation by TiO_2

photocatalysis: most have assumed pseudo-first order reactions both for photodegradation

measured in solutions [8,9,13,16,20,21] and at the air-solid interface [26,52], while in some

cases a more complex two-step model was applied [19,22,23]. Dimer degradation has rarely

been studied independently from monomer degradation. In previous studies Ghazzal *et al.* have found zero order reactions for R6G dimers [26].

It can be seen in Fig. 4f, that pseudo-first order kinetics can be used for the dimer degradation (by applying equation (1) to the experimental data), but not for the monomer degradation.

$$ln \frac{A}{A_0} = -kt \tag{1}$$

The monomer degradation results show that no linear fitting can be applied for the whole investigated time period, as initially the degradation rate is much quicker. Two different degradation rate constants can be calculated from linear fitting to the first and second interval, but these fittings use fewer points than would be satisfactory, and the goodness of fitting is still inadequate. In comparison, using the two-step model proposed by Julson and Ollis [22], a very good fitting was achieved (see Fig. 4c). Thus, the Julson-Ollis model was used for the R6G monomer degradation, which can be described as two first order processes, where the first one has a higher degradation rate.

Julson and Ollis proposed a two-step reaction model for dye degradation in porous titania on the air-solid interface under UV irradiation (see equation 2). Julson and Ollis found this model true for titania powders impregnated with different anionic dyes; while in a later publication Mills *et al.* showed that the model could also be used for titania coatings impregnated with cationic and anionic dyes, and irradiated with UV light [22,23]. In our study, it was found that the Julson-Ollis model can also be used for dye degradation under visible light (as a result of dye-sensitization), measured on mesoporous TiO_2 coatings with much lower film thickness (under 0.3 µm) than those studied by Mills *et al.* (1.8 µm).

$$dye \xrightarrow{k_1} intermediate \xrightarrow{k_2} colorless \ products \tag{2}$$
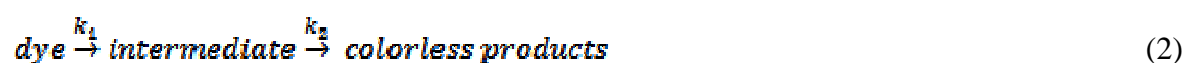
Equation (2) can be interpreted for the photodegradation of R6G with the assumption that the intermediate product is the N-dealkylated form of the R6G molecule [48–50].

The kinetics of the monomer degradation measured at the absorbance maximum around 533 nm was in good agreement with the Julson-Ollis model. The following kinetics model equation (3) was fitted to the measured A/A_0 values (Fig. 4c).

$$\frac{A}{A_0} = \left(\frac{a k_{m1}}{k_{m2}-k_{m1}}\right)\left(\exp(-k_{m1}t) - \exp(-k_{m2}t)\right) + \exp(-k_{m1}t) \tag{3}$$

where a is the ratio of α molar absorptivities: $a = \alpha$(intermediate)$/\alpha$(R6G monomer), and k_{m1}, k_{m2} are the degradation rate constants of the monomer. The equation gives an excellent fit to the measured data for R6G monomers, as seen in Fig. 4c.

The dimer degradation kinetics determined by measuring absorbance at 500 nm appeared to be more complex; the Julson-Ollis model equation did not fit to the experimental data. Instead, dimer degradation constant values were estimated by assuming pseudo-first order reactions by applying equation (1).

Fig. 5a shows that the equation for pseudo-first order kinetics, applied for the whole irradiation interval, fitted well for dimer degradation in TiO_2-CTAB and TiO_2-P123 samples, and k_d degradation constants were determined, but the model did not show good fitting in the case of TiO_2-PVP samples. In order to be able to compare the results, the degradation constants were also calculated for the first (k_{d1}) and second time periods (k_{d2}) for all sample types (the first and second time period was chosen to be before and after 30 minutes). For TiO_2-PVP samples the absorbance at the dimer peak decreased very slowly at the beginning of the degradation process: a possible explanation is that dimerization occurred as a result of the light irradiation. Although the dye molecules are adsorbed on the surface, it is possible that they are still capable of some movement. This is in accordance with the fluorescence spectroscopy measurements (see Appendix section A.4): the fluorescence anisotropy of the different R6G impregnated titania coatings was determined and compared to the anisotropy measured in dye solution. The much higher anisotropy values measured in the titania coatings

24

compared to the value measured in solution suggests that the dye molecules are adsorbed on the surface of the pores, and thus have lower mobility. In comparison, the maximum experimental value of anisotropy, called the limiting fluorescence anisotropy (r_0) of rhodamine 6G is around 0.37 (measured in propane-1,2-diol at low temperatures [47]), which is higher than the values measured for titania coatings (*ca.* 0.25).

Ghazzal *et al.* [26] found in their investigations of rhodamine 6G dye under UV irradiation on mesoporous titania films, that films with higher porosity and higher surface area led to the adsorption of a higher fraction of the dye in the monomer form, and to higher dye degradation rates. They concluded that the degradation of R6G monomers was faster than dimers, and that the monomer form is the first to be attacked during the process.

The degradation rate constants that can be seen in Fig. 5c and in Appendix Table A.1 show a similar result: a lower degradation rate was observed for the associated R6G dimer molecules than for the monomers. This difference is mostly due to the first step of the process, where the dimer degradation rate is much slower, and it was observed in experiments carried out under UV (see in the next section), and also under visible light. In some cases, during this first step, the absorbance at the dimer peak increased (Appendix Fig. A.4), suggesting that dimerization may also occur as a result of light irradiation. This process may also increase the differences observed in the monomer and dimer degradation rates.

3.3.2 UV irradiation (R6G and MB)

Photodegradation of both R6G and MB molecules under UV irradiation was studied in porous titania coatings.

3.3.2.1 Experiments with R6G

Photodegradation experiments were also carried out under UV irradiation. The same first quicker process accompanied by the monomer shift to lower wavelength values, as seen for the visible light experiments, was observed here, with the difference that this process took approximately 10 minutes, as opposed to the 30 minutes under visible light (Fig. 4b). The results show that degradation under UV irradiation happens much faster compared to the degradation rates obtained under visible light (Fig. 5b). This difference is not due to the difference of light source intensity, since the intensity of the UV light source was lower than that of the visible light source.

To better compare the degradation in UV and visible light, the degradation quantum efficiency and quantum yields can be calculated. These values were determined for the initial, first step of R6G degradation on TiO_2-P123 samples. For comparison, the same calculation was made for the TiO_2-PVP samples, which have a higher thickness, in order to determine whether the layer thickness has a significant effect on the value of the quantum yield. The detailed calculations can be seen in the Appendix section A.6. The quantum efficiency values for TiO_2-P123 samples were found to be $0.016 \pm 0.003\%$ in visible light, and $0.239 \pm 0.039\%$ in UV light. Similar values were determined for the TiO_2-PVP samples: $0.013 \pm 0.002\%$ in visible, and $0.246 \pm 0.041\%$ in UV light. The quantum yield values for TiO_2-P123 samples were estimated to be $0.037 \pm 0.006\%$ in visible, and $3.899 \pm 0.636\%$ in UV light. In comparison, the quantum yield calculated for the TiO_2-PVP samples was $0.019 \pm 0.003\%$ in visible, and $3.504 \pm 0.590\%$ in UV light, which are, once again, quite similar to those calculated for TiO_2-P123 samples.

It can be concluded from these results that the driving force for photocatalytic oxidation under UV light is significantly higher than for dye sensitization occurring under visible light. Another possible reason is that the excitation wavelength range for dye sensitization is much

smaller, as it is limited by the dye absorption peak, while all wavelengths of light can excite TiO_2 which are below a certain wavelength of UV light.

The dimer and monomer degradation kinetics were also very similar to the processes observed under visible light. The Julson-Ollis model showed good fitting to the monomer degradation results (Fig. 4d), while dimer degradation constants were estimated using pseudo-first order reaction kinetics. The first and second time period used to calculate the k_{d1} and k_{d2} dimer degradation constants was determined to be before and after 10 minutes of UV irradiation. TiO_2-PVP type coatings showed a slower monomer and dimer degradation rate during the first step (see Fig. 5d and Appendix Table A.1). Furthermore, similarly to the results from the visible light measurements, in the TiO_2-PVP samples the presence of a possible monomer-dimer organization can be observed in the kinetic curve of the dimer degradation (Fig. 5a). According to the photodegradation results obtained under visible (Fig. 5c) and UV light (Fig. 5d), the degradation rate and degradation kinetics of the adsorbed dye depend on the pore structure of the titania coatings, especially during the first step of the degradation. Dimer degradation rate was lower in the TiO_2-PVP samples than in the other coatings, especially in the first section that also showed significantly different kinetics (Fig. 5a). Monomer degradation rate was also lower in the TiO_2-PVP samples compared to the TiO_2-CTAB samples during this first section. A possible explanation for this is that the dye molecules may be able to get rid of their excited energy by movement, which is more significant in the TiO_2-PVP samples that have the widest pores. In the narrower pores of the TiO_2-CTAB samples this movement is more inhibited, and this results in a higher photodegradation rate (confined space effect). The higher pore sizes of the TiO_2-PVP coatings may also be the cause of the quicker monomer-to-dimer transformation observed in these samples. The results suggest that during photodegradation some monomer molecules form dimers: the dimerization process

occurs during the degradation, and this is why in the case of TiO_2-PVP coating a slight initial absorbance increase in the dimer peak could be observed in some cases.

Ghazzal *et al.* found that R6G photodegradation was faster in titania films with higher porosity and surface area [26]. In comparison, our results show that the titania coatings with the highest (TiO_2-P123) and lowest surface area (TiO_2-CTAB) showed similar monomer and dimer degradation rates and kinetics, while TiO_2-PVP samples, which have porosity and surface area similar to TiO_2-CTAB samples, show significantly different dimer degradation rates and kinetics. Hence, our results clearly indicate that the pore sizes have an important role in the photodegradation processes (confined space effect).
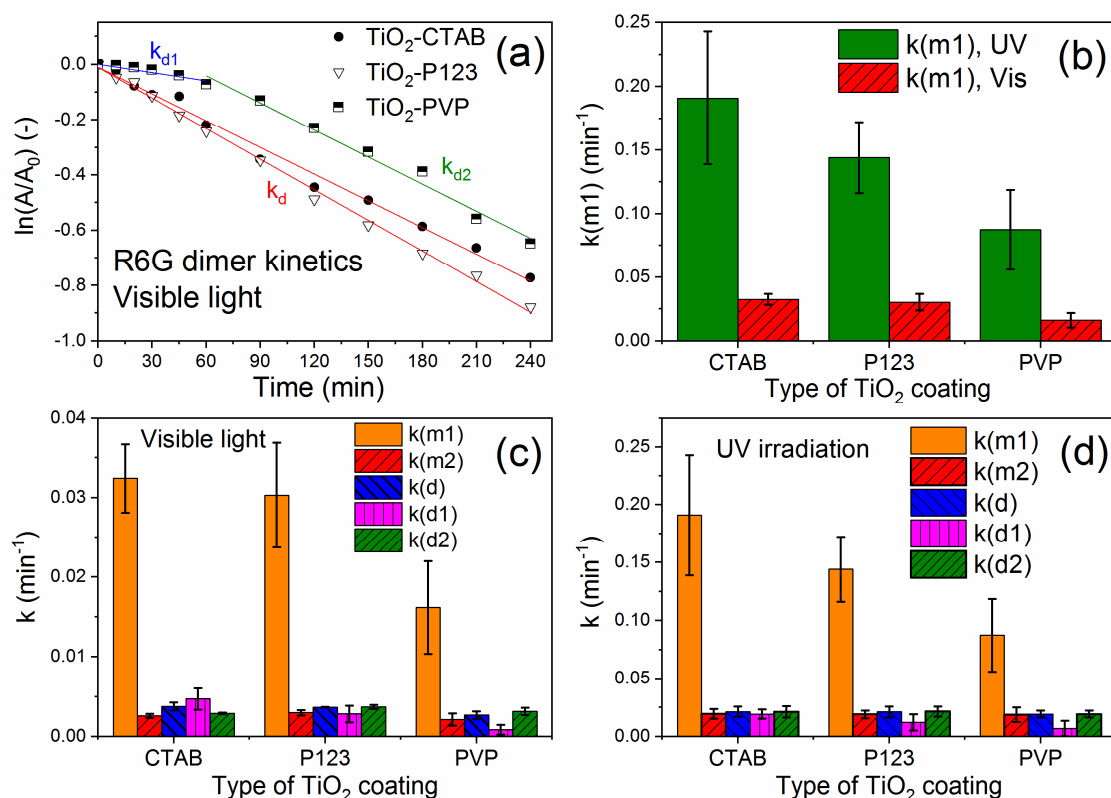

Fig. 5: R6G dimer kinetics in the different titania samples measured in visible light (A/A_0 values were measured at 500 nm) and determination of degradation rate constants (5a). Degradation rate constants of first step of monomer degradation (k_{m1}) (5b). Dimer and monomer degradation rate constants in visible (5c) and UV (5d) light. The degradation rate constants of monomer degradation (k_{m1}, k_{m2}) were determined by the Julson-Ollis model. The degradation rate constants for dimer degradation (k_d, k_{d1}, k_{d2}) were estimated as first order reactions in the whole interval (k_d), and the first (k_{d1}) and second time period (k_{d2}). Values were obtained from three or more measurements.
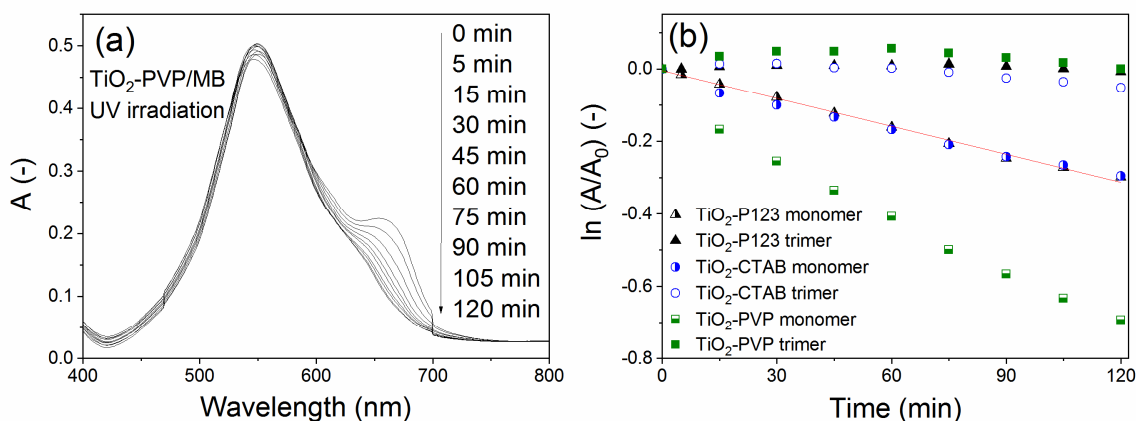
3.3.2.2 Experiments with MB

Fig. 6: Photodegradation of methylene blue under UV irradiation: discoloration of MB impregnated TiO$_2$-PVP sample during 2 h UV irradiation (6a); kinetics of photodegradation (6b).

Photodegradation study of methylene blue in porous titania coatings was carried out similarly to the previous measurements. The studied wavelength values were 655 nm for MB monomer and around 550 nm for the trimer form. Fig. 6a shows the decreasing absorbance spectra of the MB impregnated coatings under UV irradiation. During photodegradation of MB the monomer peak quickly disappears, followed by the slower decrease of the trimer peak. A slight absorbance increase at the trimer peak was observed at the beginning of the UV irradiation: it can be assumed, that monomer-to-trimer transformation was the cause of this increase. It was found that trimerization also occurs in the samples in the absence of UV irradiation during a longer time period: after the impregnation, the monomer peak slowly decreases in time while the absorbance at the trimer peak reaches a higher value. The absorbance increase occurred much more quickly under UV light than in dark, presumably the UV irradiation facilitated the trimerization reaction.

The photodegradation kinetics was found to be more complex than in the case of R6G dye. The Julson-Ollis model equation did not show good fitting to the data, most likely as a result

of the strong dye association of MB, and further trimerization process occurring during the photodegradation.

Similarly to the results found with the R6G experiments, the MB monomer's photostability appeared to be much lower than that of the associated, trimer form (Fig. 6b). The first step of the degradation is the disappearance of the monomer peak, the decrease of the absorbance at the trimer peak only starts after longer UV irradiation. Degradation constant values of the MB monomer were estimated by assuming pseudo-first order reactions by applying equation (1), as seen in Fig. 6b. The degradation rate constants for MB monomer were found to be similar for TiO_2-CTAB (0.00237 min^{-1}) and TiO_2-P123 coatings (0.00257 min^{-1}), and slightly higher for TiO_2-PVP coatings (0.00520 min^{-1}). In the case of TiO_2-PVP samples this faster decrease of the monomer peak is accompanied by an initial increase of the trimer peak, followed by a decrease after longer UV irradiation times.

The initial much faster decrease of the monomer peak is most likely caused by two factors, faster monomer degradation, and monomer-to-trimer transformation. The monomer-to-trimer formation seems to be a significant process, since it can also be observed without illumination after a longer period of time (as it was previously shown in Fig. 3d). Compared to the trimer peak increase in dark, trimerization occurs more quickly, as a result of UV irradiation, and this effect is more pronounced in the bigger pores of the TiO_2-PVP samples, presumably due to confined space effects.

4. Conclusions

It was found that associated dye forms (R6G dimers, MB trimers) accumulated in mesoporous titania coatings showed a significantly slower degradation than monomers, their photostability appears to be higher. Moreover, dimerization and trimerization processes were found to take place during photodegradation, and this behaviour depended on the pore structure of the

coatings. It was proposed that monomers and their associated forms can get rid of their excited energy through their motion in the bigger pores, while this process cannot take place in smaller pores (confined space effect). The more intensive association of monomers in the bigger pores during the photodegradation can also be explained in terms of this process. Additionally, it was shown that the degradation kinetics of R6G monomers under both UV and visible light could be described by two subsequent first order reactions. This was in good agreement with the Julson-Ollis model, which was previously found applicable for dye photodegradation under UV irradiation on the surface of TiO_2 powders. In contrast, the same model could not be applied to either for the MB monomer degradation or the degradation of associated (R6G dimer and MB trimer) forms, due to a different degradation mechanism. The results outlined above also demonstrate that photochemical processes in thin films, despite their special optical behaviour (light interference), can be reliably studied by optical spectroscopy methods.

Acknowledgements

References

[1]   Hashimoto K, Irie H, Fujishima A. TiO2 photocatalysis: A historical overview and future prospects. Japanese J Appl Physics, Part 1 Regul Pap Short Notes Rev Pap 2005;44:8269–85. doi:10.1143/JJAP.44.8269.

[2]   Kapilashrami M, Zhang Y, Liu YS, Hagfeldt A, Guo J. Probing the optical property and electronic structure of TiO_2 nanomaterials for renewable energy applications. Chem Rev 2014;114:9662–707. doi:10.1021/cr5000893.

[3]   Schneider J, Matsuoka M, Takeuchi M, Zhang J, Horiuchi Y, Anpo M, et al. Understanding TiO_2 photocatalysis: Mechanisms and materials. Chem Rev 2014;114:9919–86. doi:10.1021/cr5001892.

[4]   Shakeel Ahmad M, Pandey AK, Abd Rahim N. Advancements in the development of TiO_2 photoanodes and its fabrication methods for dye sensitized solar cell (DSSC) applications. A review. Renew Sustain Energy Rev 2017;77:89–108. doi:10.1016/j.rser.2017.03.129.

[5]   Fujishima A, Zhang X, Tryk DA. TiO_2 photocatalysis and related surface phenomena. Surf Sci Rep 2008;63:515–82. doi:10.1016/j.surfrep.2008.10.001.

[6]   Ochiai T, Fujishima A. Photoelectrochemical properties of TiO_2 photocatalyst and its applications for environmental purification. J Photochem Photobiol C Photochem Rev 2012;13:247–62. doi:10.1016/j.jphotochemrev.2012.07.001.

[7]   Hegedűs P, Szabó-Bárdos E, Horváth O, Szabó P, Horváth K. Investigation of a TiO_2 photocatalyst immobilized with poly(vinyl alcohol). Catal Today 2017;284:179–86. doi:10.1016/j.cattod.2016.11.050.

[8]   Konstantinou IK, Albanis TA. TiO_2-assisted photocatalytic degradation of azo dyes in aqueous solution: Kinetic and mechanistic investigations: A review. Appl Catal B Environ 2004;49:1–14. doi:10.1016/j.apcatb.2003.11.010.

[9]   Song XM, Wu JM, Yan M. Photocatalytic degradation of selected dyes by titania thin films with various nanostructures. Thin Solid Films 2009;517:4341–7. doi:10.1016/j.tsf.2009.02.132.

[10]   Justh N, Berke B, László K, Bakos LP, Szabó A, Hernádi K, et al. Preparation of graphene oxide/semiconductor oxide composites by using atomic layer deposition. Appl Surf Sci 2018;453:245–51. doi:10.1016/j.apsusc.2018.05.064.

[11]   Mérai L, Varga N, Deák Á, Sebők D, Szenti I, Kukovecz Á, et al. Preparation of photocatalytic thin films with composition dependent wetting properties and self-healing ability. Catal Today 2018. doi:10.1016/j.cattod.2018.10.015.

[12]   Grätzel M. Dye-sensitized solar cells. J Photochem Photobiol C Photochem Rev 2003;4:145–53. doi:10.1016/S1389-5567(03)00026-1.

[13]   Lachheb H, Puzenat E, Houas A, Ksibi M, Elaloui E, Guillard C, et al. Photocatalytic degradation of various types of dyes (Alizarin S) in water by UV-irradiated titania.

Appl Catal B Environ 2002;39:75–90. doi:10.1002/mmnd.193819380103.

[14]   Ajmal A, Majeed I, Malik RN, Idriss H, Nadeem MA. Principles and mechanisms of photocatalytic dye degradation on TiO2 based photocatalysts: A comparative overview. RSC Adv 2014;4:37003–26. doi:10.1039/c4ra06658h.

[15]   Akpan UG, Hameed BH. Parameters affecting the photocatalytic degradation of dyes using TiO2-based photocatalysts: A review. J Hazard Mater 2009;170:520–9. doi:10.1016/j.jhazmat.2009.05.039.

[16]   Zhang F, Zhao J, Shen T, Hidaka H, Pelizzetti E, Serpone N. TiO2-assisted photodegradation of dye pollutants II. Adsorption and degradation kinetics of eosin in TiO2 dispersions under visible light irradiation. Appl Catal B Environ 1998;15:147–56. doi:10.1016/S0926-3373(97)00043-X.

[17]   Kun R, Balázs M, Dékány I. Photooxidation of organic dye molecules on TiO2and zinc-aluminum layered double hydroxide ultrathin multilayers. Colloids Surfaces A Physicochem Eng Asp 2005;265:155–62. doi:10.1016/j.colsurfa.2005.02.044.

[18]   Wang JC, Lou HH, Xu ZH, Cui CX, Li ZJ, Jiang K, et al. Natural sunlight driven highly efficient photocatalysis for simultaneous degradation of rhodamine B and methyl orange using I/C codoped TiO_2 photocatalyst. J Hazard Mater 2018;360:356–63. doi:10.1016/j.jhazmat.2018.08.008.

[19]   Bergamini RBM, Azevedo EB, Araújo LRR de. Heterogeneous photocatalytic degradation of reactive dyes in aqueous TiO_2 suspensions: Decolorization kinetics. Chem Eng J 2009;149:215–20. doi:10.1016/j.cej.2008.10.019.

[20]   Dostanić J, Grbić B, Radić N, Stefanov P, Šaponjić Z, Buha J, et al. Photodegradation of an azo pyridone dye using TiO2films prepared by the spray pyrolysis method. Chem Eng J 2012;180:57–65. doi:10.1016/j.cej.2011.10.100.

[21]   Baran W, Makowski A, Wardas W. The effect of UV radiation absorption of cationic and anionic dye solutions on their photocatalytic degradation in the presence TiO_2. Dye Pigment 2008;76:226–30. doi:10.1016/j.dyepig.2006.08.031.

[22]   Julson AJ, Ollis DF. Kinetics of dye decolorization in an air-solid system. Appl Catal B Environ 2006;65:315–25. doi:10.1016/j.apcatb.2005.12.021.

[23]   Mills A, Sheik M, O'Rourke C, McFarlane M. Adsorption and photocatalysed destruction of cationic and anionic dyes on mesoporous titania films: Reactions at the air-solid interface. Appl Catal B Environ 2009;89:189–95. doi:10.1016/j.apcatb.2008.11.029.

[24]   Strataki N, Bekiari V, Stathatos E, Lianos P. Effect of aggregation of dyes adsorbed on

nanocrystalline titania films on the efficiency of photodegradation. J Photochem Photobiol A Chem 2007;191:13–8. doi:10.1016/j.jphotochem.2007.03.023.

[25] Strataki N, Bekiari V, Lianos P. Study of the conditions affecting dye adsorption on titania films and of their effect on dye photodegradation rates. J Hazard Mater 2007;146:514–9. doi:10.1016/j.jhazmat.2007.04.052.

[26] Ghazzal MN, Kebaili H, Joseph M, Debecker DP, Eloy P, De Coninck J, et al. Photocatalytic degradation of Rhodamine 6G on mesoporous titania films: Combined effect of texture and dye aggregation forms. Appl Catal B Environ 2012;115–116:276–84. doi:10.1016/j.apcatb.2011.12.016.

[27] Ghori MZ, Veziroglu S, Henkel B, Vahl A, Polonskyi O, Strunskus T, et al. A comparative study of photocatalysis on highly active columnar TiO_2 nanostructures in-air and in-solution. Sol Energy Mater Sol Cells 2018;178:170–8. doi:10.1016/j.solmat.2018.01.019.

[28] Vogel R, Meredith P, Harvey MD, Rubinsztein-Dunlop H. Absorption and fluorescence spectroscopy of rhodamine 6G in titanium dioxide nanocomposites. Spectrochim Acta - Part A Mol Biomol Spectrosc 2004;60:245–9. doi:10.1016/S1386-1425(03)00218-X.

[29] Avnir D, Levy D, Reisfeld R. The nature of the silica cage as reflected by spectral changes and enhanced photostability of trapped rhodamine 6G. J Phys Chem 1984;88:5956–9. doi:10.1021/j150668a042.

[30] Singh S, Kanetkar VR, Sridhar G, Muthuswamy V, Raja K. Solid-state polymeric dye lasers. J Lumin 2003;101:285–91. doi:10.1016/S0022-2313(02)00571-9.

[31] Tatikolov AS. Polymethine dyes as spectral-fluorescent probes for biomacromolecules. J Photochem Photobiol C Photochem Rev 2012;13:55–90. doi:10.1039/c2cc31405c.

[32] Albert E, Cotolan N, Nagy N, Sáfrán G, Szabó G, Mureşan LM, et al. Mesoporous silica coatings with improved corrosion protection properties. Microporous Mesoporous Mater 2015;206:102–13. doi:10.1016/j.micromeso.2014.12.021.

[33] Chen Z, Tang YJ, Xie TT, Chen Y, Li YQ. Fluorescence spectral properties of rhodamine 6G at the silica/water interface. J Fluoresc 2008;18:93–100. doi:10.1007/s10895-007-0241-x.

[34] Macedo J de S, da Costa Júnior NB, Almeida LE, Vieira EF da S, Cestari AR, Gimenez I de F, et al. Kinetic and calorimetric study of the adsorption of dyes on mesoporous activated carbon prepared from coconut coir dust. J Colloid Interface Sci 2006;298:515–22. doi:10.1016/j.jcis.2006.01.021.

[35]   Novotna P, Krysa J, Maixner J, Kluson P, Novak P. Photocatalytic activity of sol-gel
       TiO2 thin films deposited on soda lime glass and soda lime glass precoated with a SiO2
       layer. Surf Coatings Technol 2010;204:2570–5. doi:10.1016/j.surfcoat.2010.01.043.

[36]   Kócs L, Albert E, Tegze B, Kabai-Faix M, Major C, Szalai A, et al. Silica Sol-gel
       coatings with improved light transmittance and stability. Period Polytech Chem Eng
       2018;62:21–31. doi:10.3311/PPch.10550.

[37]   Volentiru E, Nyári M, Szabó G, Hórvölgyi Z, Murẹan LM. Silica sol - Gel protective
       coatings against corrosion of zinc substrates. Period Polytech Chem Eng 2014;58:61–6.
       doi:10.3311/PPch.7302.

[38]   Hild E, Deák A, Naszályi L, Sepsi Ö, Ábrahám N, Hórvölgyi Z. Use of the optical
       admittance function and its WKB approximation to simulate and evaluate transmittance
       spectra of graded-index colloidal films. J Opt A Pure Appl Opt 2007;9:920–30.
       doi:10.1088/1464-4258/9/10/023.

[39]   Heller W. Remarks on refractive index mixture rules. J Phys Chem 1965;69:1123–9.
       doi:10.1021/j100888a006.

[40]   Albert E, Albouy PA, Ayral A, Basa P, Csík G, Nagy N, et al. Antibacterial properties
       of Ag–TiO2 composite sol–gel coatings. RSC Adv 2015;5:59070–81.
       doi:10.1039/C5RA05990A.

[41]   Sáfrán G, Szász N, Sáfrán E. Two-In-one sample preparation for plan-VIew TEM.
       Microsc Res Tech 2015;78:599–602. doi:10.1002/jemt.22513.

[42]   Lu Y, Ganguli R, Drewien CA, Anderson MT, Brinker CJ, Gong W, et al. Continuous
       formation of supported cubic and hexagonal mesoporous films by sol–gel dip-coating.
       Nature 1997;389:364–8. doi:10.1038/38699.

[43]   Albert E, Basa P, Deák A, Németh A, Osváth Z, Sáfrán G, et al. Introducing
       nanoscaled surface morphology and percolation barrier network into mesoporous silica
       coatings. RSC Adv 2015;5:60041–53. doi:10.1039/c5ra09357k.

[44]   Bain AJ, Chandna P, Butcher G, Bryant J. Picosecond polarized fluorescence studies of
       anisotropic fluid media. II. Experimental studies of molecular order and motion in jet
       aligned rhodamine 6G and resorufin solutions. J Chem Phys 2000;112:10435–49.
       doi:10.1063/1.481679.

[45]   Cenens J, Schoonheydt RA. Visible Spectroscopy of Methylene Blue on Hectorite,
       Laponite B, and Barasym in Aqueous Suspension. Clays Clay Miner 1988;36:214–24.
       doi:10.1346/CCMN.1988.0360302.

[46]   Braswell E. Evidence for trimerization in aqueous solutions of methylene blue. J Phys

Chem 1968;72:2477–83. doi:10.1021/j100853a035.

[47] Johansson LB-A. Limiting Fluorescence Anisotropies of Perylene and Xanthene Derivatives. J Chem Soc Faraday Trans 1990;86:2103–7. doi:10.1039/FT9908602103.

[48] Fan Y, Chen G, Li D, Luo Y, Lock N, Jensen AP, et al. Highly selective deethylation of rhodamine B on TiO2 prepared in supercritical fluids. Int J Photoenergy 2012;2012. doi:10.1155/2012/173865.

[49] Watanabe T, Takizawa T, Honda K. Photocatalysis through excitation of adsorbates. 1. Highly efficient N-deethylation of rhodamine B adsorbed to cadmium sulfide. J Phys Chem 1977;81:1845–51. doi:10.1021/j100534a012.

[50] Rasheed T, Bilal M, Iqbal HMN, Hu H, Zhang X. Reaction Mechanism and Degradation Pathway of Rhodamine 6G by Photocatalytic Treatment. Water Air Soil Pollut 2017:228: 291. doi:10.1007/s11270-017-3458-6.

[51] Zhao J, Chen C, Ma W. Photocatalytic degradation of organic pollutants under visible light irradiation. Top Catal 2005;35:269–78. doi:10.1007/s11244-005-3834-0.

[52] Ollis D. Kinetics of photocatalyzed film removal on self-cleaning surfaces: Simple configurations and useful models. Appl Catal B Environ 2010;99:478–84. doi:10.1016/j.apcatb.2010.06.029.

[53] Allain E, Besson S, Durand C, Moreau M, Gacoin T, Boilot JP. Transparent mesoporous nanocomposite films for self-cleaning applications. Adv Funct Mater 2007;17:549–54. doi:10.1002/adfm.200600197.

[54] Mills A, Lepre A, Elliott N, Bhopal S, Parkin IP, O'Neill SA. Characterisation of the photocatalyst Pilkington Activ[TM]: A reference film photocatalyst? J Photochem Photobiol A Chem 2003;160:213–24. doi:10.1016/S1010-6030(03)00205-3.